Eurasian
Chemical
Communications

◀)) SAMI

FULL PAPER

Molecular docking and three-dimensional quantitative structure-activity relationship studies on 5-HT6 receptor inhibitors and design of new compounds

Eslam Pourbasheer[a],* iD |**Reza Aalizadeh[b]** |**Mohammad Reza Ganjali[c,d]**

[a]*Department of Chemistry, Faculty of Science, University of Mohaghegh Ardabili, P.O. BOX 179, Ardabil, Iran*

[b]*Laboratory of Analytical Chemistry, Department of Chemistry, University of Athens, Panepistimiopolis Zografou, 15771 Athens, Greece*

[c]*Center of Excellence in Electrochemistry, Faculty of Chemistry, University of Tehran, Tehran, Iran*

[d]*National Institute of Genetic Engineering and Biotechnology (NIGEB), Tehran, Iran*

CoMFA and CoMSIA methods were used to perform 3D quantitative structure-activity relationship (3D-QSAR) evaluation and molecular docking, of 5-HT$_6$ receptor inhibitors. The CoMFA model performed on training set in biases of alignment with suitable statistical parameters (q^2= 0.556, r^2 = 0.836, F= 26.334, SEE=0.171). The best prediction for 5-HT$_6$ receptor inhibitors was obtained by CoMFA (after focusing region) model with highest predictive ability (q^2= 0.599, r^2 = 0.857, F= 30.853, SEE=0.160) in biases of the same alignment. Using the same alignment, a consistent CoMSIA model was obtained (q^2= 0.580, r^2 = 0.752, F= 34.361, SEE=0.201) from the three combinations. To evaluate the prediction capability of the CoMFA and CoMSIA models, a test set of 9 compounds was used so that they could show the good predictive r^2 values for CoMFA, CoMFA (after focusing region), and CoMSIA models, 0.554, 0.473, and 0.670, respectively. The obtained contour maps form models were used to identify the structural features responsible for the biological activity to design potent 5-HT$_6$ receptor inhibitors. Molecular docking analysis along with the CoMSIA model could reveal the significant role of hydrophobic characteristics in increasing the inhibitors potency. Using the results, some new compounds were designed which showed the higher inhibitory activities as 5-HT$_6$ receptor inhibitors.

*Corresponding Author:

Eslam Pourbasheer

Email: e.pourbasheer@uma.ac.ir

Tel.: +98-45-31505204

Introduction

Monoamine neurotransmitter serotonin (5-hydrox-ytryptamine) is located in central and peripheral nervous systems, [1,2] and as a local hormone in numerous other tissues [1,3-5]. It plays a crucial role in different central and physiological functions, including motor, sensory, [5] cognitive, sleep, behavior, and appetite [6,7]. The 5-HT families are also engaged in neuropsychiatric [5,8] and neurodegenerative disorders like depression,

[7] Parkinson's, and Alzheimer's diseases [9], anxiety and migraine [6,9,10]. 5-HT family consists of seven main subtypes (5-HT$_1$, 5-HT$_2$, 5-HT$_3$, 5-HT$_4$, 5-HT$_5$, 5-HT$_6$, and 5-HT$_7$) [2, 11]. Among the 5-HT receptors, the 5-HT$_6$ receptor shows a moderate affinity for serotonin, and a variety of antipsychotic and antidepressant drugs implemented the higher affinity for this receptor [9]. An increasing interest is attracted to the 5-HT$_6$ receptor due to the evidence that it plays a significant impact on pain modulation, [5] seizures, [7] drug abuse,

and the sleep-wake cycle [12]. Since inhibition of this receptor might increase the acetylcholine release in the frontal cortex, it could be a good target to treat the episodic memory deficits in schizophrenia [8,13]. Regarding this issue, several approaches [14-16] were carried out to design new selective, and 5-HT$_6$ inhibitors with fewer side effects for schizophrenic patients.

Many studies have been developed to design new potent 5-HT$_6$ receptor antagonists [14-16]. Recently, Nirogi *et al.,* [17] could design and suggest some novel compounds as 5-HT$_6$ receptor inhibitors. These compounds were derived from tetrahydrocarbazole moiety. Subsequently, they suggested two active sites for assessing the impact of different groups on affinity for *in vitro* binding. The newly developed inhibitors could show striking binding affinity and inhibitory activity. However, understanding the mixed effect of various groups present in substituents requires more studies.

The novel compounds should be evaluated in bio-materials obtained from human or calf origin, to understand the bio-activity of each molecule. The tests are, however, costly, time intensive and put lab technicians at health risk. The computer-aided design methods, constitute a safe and low-cost pathway for obtaining the activity of each compound based on its chemical structure. Quantitative structure- activity relationships (QSAR) is a widely used computational method in drug design, [18-21] which uses molecular properties a basis for predicting the biological activities of compounds [22-25]. The method can also be used to construct a model to predict and identify the main features controlling the inhibitory properties, but it does not consider the three-dimensional structure or chirality of drug molecules. Therefore, this method led to develop a novel method, namely; three-dimensional quantitative structure activity relationship (3D-QSAR) [26, 27]. Using 3D-QSAR allows the correlation between the biological activities

and their 3D structures to derive indirect binding information [28-30]. The predictive 3D-QSAR model can be built based on the so-called comparative molecular field analysis (CoMFA)[31] and the comparative molecular similarity indices analysis (CoMSIA)[32] methods. An outcome of CoMFA and CoMSIA is a graphical result called the contour map. The former technique notes the steric and electrostatic properties of the molecule in a 3D Cartesian space, [31] while the latter uses similarity indices, which can be turned into contour maps including hydrophobic and hydrogen-bonding donor and acceptor [32]. The effect of chemical features on the biological behavior of molecules can be obtained using these additional fields.

Here, docking and 3D-QSAR analyses were used on a series of 5-HT$_6$ receptor inhibitors [33, 34]. CoMFA and CoMSIA methods were used to obtain the contour maps to describe the effects of physicochemical and structural factors on 5-HT$_6$ receptor inhibition activity. Molecular docking was further used to investigate the interactions of protein and ligand, and the suitable conformation of compounds in the prepared protein.

Methodology

Data set

The molecular modeling study was performed using a set of 48 compounds as 5-HT$_6$ receptor inhibitors with reported binding affinity potency was taken from literature.[17] The pK$_i$ values were used as dependent variables to form the CoMFA and CoMSIA analyses. The binding affinity activities as K$_i$ (nM) values for all compounds were converted into the logarithmic scale [pK$_i$ (M)]. To reach distribution of the biological data over the whole set, and concerning the diversity of their chemical structures, the data set was randomly divided in to training and test sub-sets. A 38-molecule training set (80%) was used to obtain the 3D-QSAR models, while the model validation test set comprised of 9

compounds (20%). A summary of the structures of all molecules and their bioactivity levels is listed in Table 1.

Molecular modeling and alignment

The molecular modeling package SYBYL 7.3 was used to obtain the 3D molecular structures.[35] Tripos force field with a dependent dielectric and the Powell conjugate gradient algorithm convergence criterion of 0.01 kcal/mol Å were used for the energy minimization [36] and Gasteiger-Hückel method [37] was used to determine the partial atomic charges. The choice of the template molecule is a key step in the 3D-QSAR analysis, because the alignment of test molecules with the reference molecule greatly influences the prediction ability and strength of models. The compound with the highest activity is usually chosen as the reference, and the rest of the molecules are aligned according to the common structure. The most active and reference molecule in this work, was molecule **19**, and the rest of the compounds were aligned with reference to it to obtain the 3D-QSAR analysis. Figures 1 and 2 show the structure of the template molecule with a bolded common substructure and the aligned molecules, respectively.
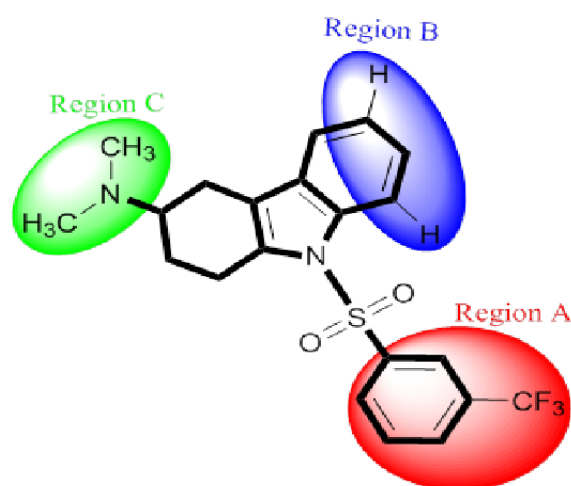

FIGURE 1 Structure of template compound (molecule 19). The three regions A, B, and C depicted and common substructure is in bold
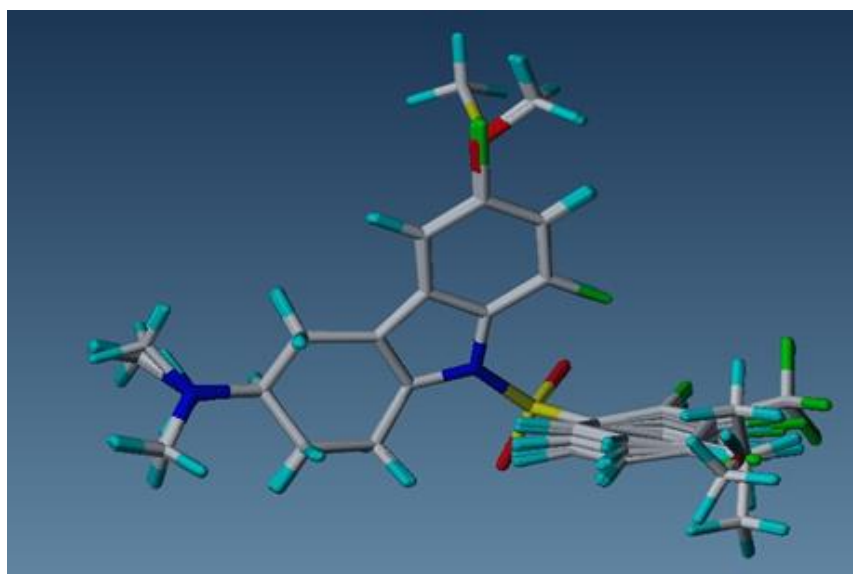

FIGURE 2 Alignment of training and test set compounds on compound 19

Molecular docking

Being a well-known procedure for drug assessment, molecular docking can yield the appropriate conformations of a compound in protein binding sites [38-40]. To simulate the acceptable conformation of a compound with the lowest energy level, and subsequently understand the existing interactions between tetrahydrocarbazole derivatives and 5-HT$_6$ receptor, docking was performed with the help of AutoDock 4.2. [41] The protein complexes were chosen from http://www.rcsb.org with a PDB ID of 1U19, [42] based on a 2.2 Å resolution X-ray crystal structure of bovine rhodopsin and is highly similar to the experiment set [42]. Prior to docking, the protein was treated by removing the water molecules, and flowing by adding polar H atoms and Kollman charges to the structure of the protein. The respective grid box size and grid space of 60 × 60 × 60 Å and 0.375 Å were defined to include the binding site, for the docking. Consequently, the most highly active compound in the data set flexibly docked into the active binding site. During the docking procedure, the ten best ligand conformations of each compound were selected based on the dock score value, followed by evaluating the interactions for the proper orientation with the minimum binding energy. Ligand Scout 3.03 was used for performing the pharmacophore studies [43].

CoMFA procedure

The 3D-QSAR predictive model was constructed using the CoMFA method on the aligned molecules. The steric (Lennard-Jones) and electrostatic (Coulombic) potential fields were calculated in a 3D cubic lattice with a 2.0 Å grid spacing and extended at least 4.0 Å beyond the Van der Waals forces around the aligned molecules in all directions, by the CoMFA method. The steric and electrostatic fields (with a +1.0 charge and the Van der Waals radius of 1.52 Å) were generated using an sp3 hybridized carbon as the probe. To enhance the model efficiencies and noise, for the columns to have less energy variance, the column filtering was set to 1.0 kcal/mol, and incompatible energy variance were eliminated. A cut-off energy value of 30 kcal/mol was chosen as the steric and electrostatic contributions to lower the electrostatic energies and minimize the large steric effects. The CoMFA region focusing, which includes assigning weights to lattice points in a CoMFA region, was used to improve or reduce the point contributions in the analyses. The StDev coefficients were also used as alternative weighing factors, further to grid spacing, to obtain the better results.

CoMSIA procedure

CoMSIA was used in the same lattice box of CoMFA, to help determine the similarity indices of the compounds. The method can provide information on the steric and electrostatic fields, as well as on hydrophobic, hydrogen bond donor, and acceptor descriptors. The five CoMSIA descriptors were based on the standard settings (charge=+1, hydrophobicity=+1, hydrogen bond donor/acceptor at each lattice=1, and grid spacing 2.0Å) of an sp3 carbon probe [32,44]. Among these descriptors, the steric indices correspond to the 3rd power of the atomic radii, the electrostatic indices are determined based on the partial charges of the atoms; the hydrophobic fields are obtained from atom-based parameters proposed by Viswanadhan *et al.* [45], and rule-based techniques using from experimental data were the source of hydrogen bond donor and acceptor indices [44]. The similarity indices of the molecules and the probe atom were evaluated based on the Gaussian function, and then the mutual distance was evaluated between them. A column filtering value of 1.0 kcal/mol was applied to improve the predictive capability of the model.

Partial least square analysis and validations

The partial least square method (PLS), [46] was employed to estimate the minimum set of grid points, which linearly correlates the CoMFA and CoMSIA fields to the pK_i values, in constructing the three-dimensional QSAR model [47]. To evaluate the prediction capability of the built PLS model, cross-validation based on the leave-one-out (LOO) approach was performed. [46,47] The analysis of being cross-validated is a method, where one molecule was eliminated from the set, for its activity to be projected solely by the model obtained from the rest. This trend was rendered for each molecule to obtain the cross-validation correlation coefficient (q^2), as a good indicator of the prediction capability of the model. The efficiency of the 3D-QSAR model was improved, and noise (i.e. the section of the molecule not involved in bioactive behavior, [48] were minimized by setting the column filtering value (σ) at 1.0 kcal/mol. The optimal number of components, with the minimum standard error of predictions (SEP), was obtained by combining the PLS model with cross-validation. The variability of the parameters in a final model can be estimated from cross-validated correlation coefficients.

The model was finally established based on the optimum component number through non-cross-validation treatment. The robustness and statistical validity was assessed using squared correlation (r^2) the cross-validated correlation (q^2) coefficients. The model's stability and strength were studied through leave-many-out (LMO) cross-validation, and bootstrapping treatments was confirmed based on the average value of 100 runs from every cross-validation. Each model was subjected to the statistical calculation to determine the one with the minimal standard error of predictions (SEP), as well as the maximum squared correlation coefficient (r^2) and F values. The compounds in the 9-member set were used to test the external prediction

capability of the models, and the predictive correlation coefficient (r^2 pred) was determined using the models.
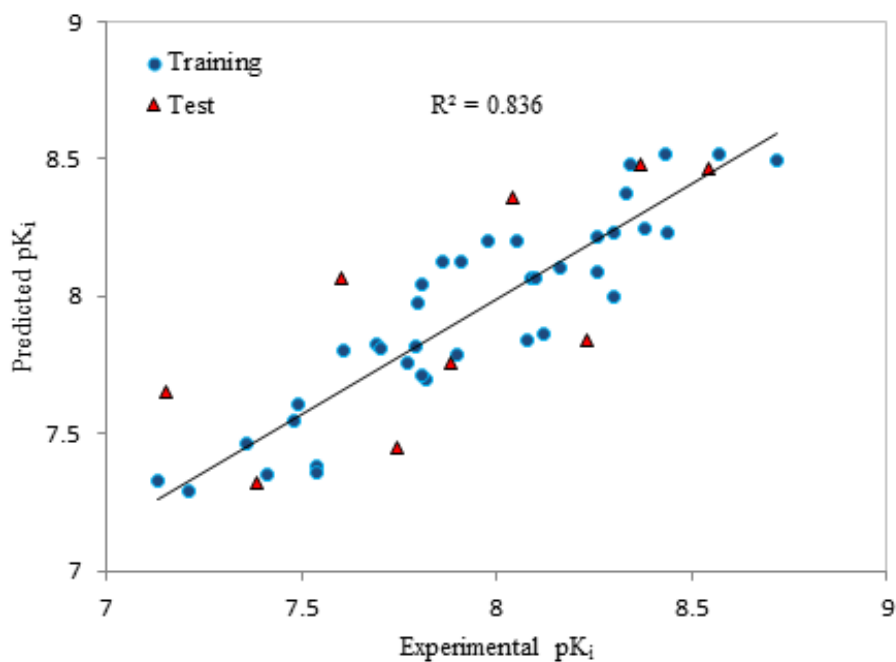
Results and discussion

CoMFA analysis

The CoMFA model was developed using a 38-compound training set, and a 9-compound external test set for further assessing the applicability and reliability of the model. Likewise, the structures of compounds, their binding activity, and affinity were correlated using the PLS method. The statistical factors associated with the acceptance of a model for predicting of the unknown compounds are presented in Table 2. The cross-validated q^2 of the developed CoMFA-1 model by 6 components was 0.556. The number of components leading to the highest q^2 was considered optimal. An r^2 of 0.836, F = 26.334, which is conventional, was obtained from non-cross-validated PLS analysis for 6 components, and the standard error for the estimated value (SEE) was 0.171. As can be seen from Table 2, the contributions of the steric and electrostatic factors in the model developed based on the CoMFA-1 model were 74.1% and 25.9% of variance. The high bootstrapping value was determined as 0.903. The high F, bootstrapping, q^2 and r^2 values, and the low SEE were indicative of the considerable prediction ability of the developed model. The pK_i values predicted by the CoMFA-1 model are presented in Table 1 and the correlation between theoretical and experimental pK_i values can be seen in Figure 3(A).
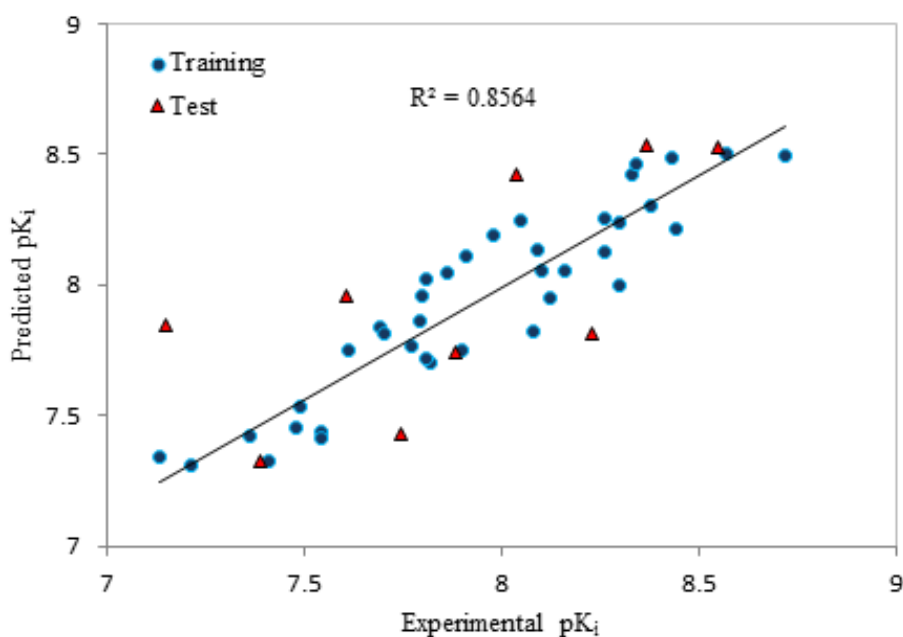
The CoMFA-1 model can be further improved by the so-called region focusing on CoMFA, which is based on assigning weights to lattice points in a CoMFA region. This way, the analytical contribution of the points, and subsequently the q^2 value are enhanced. Through this procedure, another model (i.e. CoMFA-2) was obtained with significantly improved statistical parameters. As provided

in Table 2, q^2 changed from 0.556 to 0.599, as did the r^2 value (to 0.857), indicating a good improvement for the same number of components. Accordingly, the bootstrapping of the new model significantly increased to (0.910), F (30.853), and SEE dropped to 0.160. The contributions of the steric and electrostatic fields according to CoMFA-2
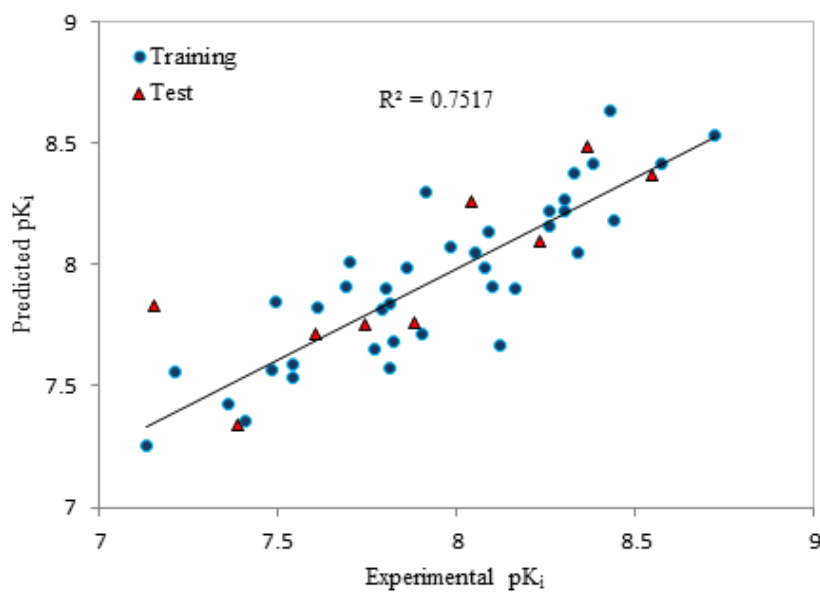
were % 70.0 and % 30.0 of variance. Figure 4 shows the electrostatic and steric fields according to CoMFA-2 (i.e. after region focusing). The pK_i values obtained using CoMFA-2 are listed in Table 1, and the correlation of the CoMFA-2 theoretical and experimental pIC_{50} values are depicted in Figure 3B.

(A)
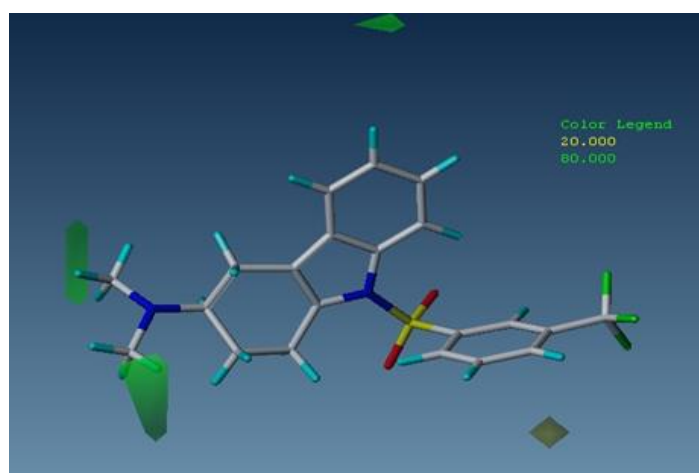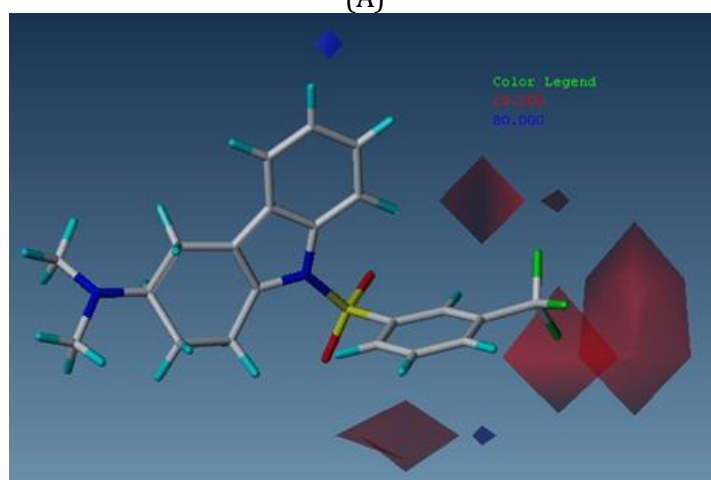

(B)

(C)

FIGURE 3 Plot of experimental against predicted pIC$_{50}$ by CoMFA (A), CoMFA after region focusing (B), and CoMSIA (C)
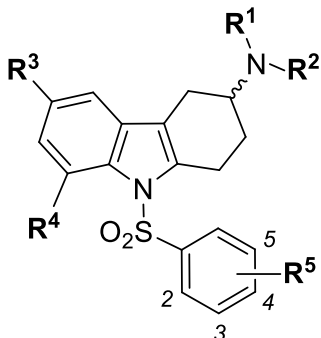

(A)

(B)

FIGURE 4 Contour maps of CoMFA: steric (A) and electrostatic (B) based on compound **19**

SAMI — Eurasian Chemical Communications

TABLE 1 Chemical structures of 5-HT$_6$ receptor inhibitors with their experimental and predicted activities

No.	R$_1$	R$_2$	R$_3$	R$_4$	R$_5$	Exp. (pK$_i$)	CoMFA-1	CoMFA-2	CoMSIA
1	CH$_3$	CH$_3$	H	H	H	8.05	8.20	8.25	8.05
2[b]	CH$_3$	CH$_3$	Br	H	H	8.74	-	-	-
3	CH$_3$	CH$_3$	Cl	H	H	7.79	7.82	7.87	7.82
4	CH$_3$	CH$_3$	F	H	H	7.80	7.97	7.96	7.90
5	CH$_3$	CH$_3$	OCH$_3$	H	H	8.26	8.22	8.25	8.16
6	CH$_3$	CH$_3$	SCH$_3$	H	H	8.34	8.48	8.47	8.05
7	CH$_3$	CH$_3$	F	F	H	8.10	8.06	8.06	7.91
8	CH$_3$	CH$_3$	H	H	4-Br	7.81	7.71	7.72	7.57
9[a]	CH$_3$	CH$_3$	Cl	H	4-Br	7.39	7.32	7.33	7.34
10	CH$_3$	CH$_3$	F	H	4-Br	7.36	7.46	7.42	7.43
11	CH$_3$	CH$_3$	OCH$_3$	H	4-Br	7.82	7.7	7.70	7.68
12	CH$_3$	CH$_3$	H	H	4-F	7.90	7.79	7.75	7.72
13	CH$_3$	CH$_3$	F	H	4-F	7.48	7.55	7.45	7.57
14	CH$_3$	CH$_3$	OCH$_3$	H	4-F	7.61	7.80	7.75	7.83
15[a]	CH$_3$	CH$_3$	SCH$_3$	H	4-F	7.60	8.07	7.96	7.71
16	CH$_3$	CH$_3$	H	H	3-Cl	8.38	8.24	8.30	8.42
17	CH$_3$	CH$_3$	F	H	3-Cl	8.30	8.00	8.00	8.27
18	CH$_3$	CH$_3$	SCH$_3$	H	3-Cl	8.57	8.52	8.50	8.41
19	CH$_3$	CH$_3$	H	H	3-CF$_3$	8.72	8.50	8.50	8.53
20	CH$_3$	CH$_3$	Br	H	3-CF$_3$	8.26	8.09	8.12	8.22
21	CH$_3$	CH$_3$	Cl	H	3-CF$_3$	7.91	8.13	8.11	8.30
22	CH$_3$	CH$_3$	OCH$_3$	H	3-CF$_3$	8.43	8.51	8.49	8.64
23[a]	CH$_3$	CH$_3$	H	H	2-Br	8.55	8.46	8.53	8.37
24	CH$_3$	CH$_3$	Cl	H	2-Br	8.09	8.06	8.13	8.13
25	CH$_3$	CH$_3$	F	H	2-Br	8.30	8.23	8.24	8.22
26[a]	CH$_3$	CH$_3$	OCH$_3$	H	2-Br	8.37	8.48	8.53	8.48
27[a]	CH$_3$	CH$_3$	H	H	2-Cl	8.04	8.36	8.42	8.26
28	CH$_3$	CH$_3$	OCH$_3$	H	2-Cl	8.33	8.37	8.42	8.37
29	CH$_3$	CH$_3$	H	H	2-F	7.98	8.20	8.19	8.07
30	CH$_3$	CH$_3$	OCH$_3$	H	2-F	8.44	8.24	8.21	8.18
31	CH$_3$	CH$_3$	H	H	4-CH$_3$	8.08	7.844	7.83	7.99
32[a]	CH$_3$	CH$_3$	Cl	H	4-CH$_3$	7.74	7.45	7.43	7.75
33	CH$_3$	CH$_3$	F	H	4-CH$_3$	7.49	7.61	7.53	7.85
34	CH$_3$	CH$_3$	SCH$_3$	H	4-CH$_3$	7.86	8.13	8.05	7.99
35[a]	CH$_3$	CH$_3$	OCH$_3$	H	4-CH$_3$	8.23	7.84	7.81	8.10
36	CH$_3$	CH$_3$	Br	H	4-CH(CH$_3$)$_2$	8.12	7.87	7.95	7.67
37	CH$_3$	CH$_3$	F	H	4-CH(CH$_3$)$_2$	7.81	8.04	8.02	7.84
38	CH$_3$	CH$_3$	H	H	4-OCH$_3$	7.69	7.82	7.84	7.91
39	CH$_3$	CH$_3$	Br	H	4-OCH$_3$	7.54	7.38	7.44	7.59
40	CH$_3$	CH$_3$	OCH$_3$	H	4-OCH$_3$	7.70	7.81	7.82	8.01
41	CH$_3$	CH$_3$	SCH$_3$	H	4-OCH$_3$	8.16	8.10	8.06	7.90
42[a]	CH$_3$	CH$_3$	Br	H	2-Cl, 5-CF$_3$	7.15	7.65	7.85	7.83

43	CH$_3$	CH$_3$	Br	H	2,3,4-trifluoro	7.21	7.29	7.31	7.56
44	CH$_3$	CH$_3$	Br	H	3,4- difluoro	7.54	7.36	7.41	7.53
45	H	CH$_3$	H	H	3-CF$_3$	7.77	7.76	7.76	7.65
46[a]	H	CH$_3$	OCH$_3$	H	3-CF$_3$	7.88	7.76	7.74	7.76
47	H	H	H	H	3-CF$_3$	7.13	7.33	7.34	7.26
48	H	H	OCH$_3$	H	3-CF$_3$	7.41	7.35	7.33	7.36

[a]Test set
[b]Outlier

TABLE 2 Statistical results of CoMFA and best CoMSIA models

PLS statistics	CoMFA-1	CoMFA-2 (after region focusing)	CoMSIA (Best model)
LOO cross q^2 /SEP[a]	0.556/0.281	0.599/0.267	0.580/0.327
Group cross q^2 /SEP	0.567/0.278	0.586/0.274	0.550/0.270
Non-validated r^2 /SEE[b]	0.836/0.171	0.857/0.160	0.752/0.201
F	26.334	30.853	34.361
r$^2_{bootstrap}$	0.903±0.029	0.910±0.033	0.885±0.038
S $_{bootstrap}$	0.131±0.054	0.122±0.069	0.141±0.080
Optimal components	6	6	3
r$^2_{test}$	0.554	0.473	0.670
Field distribution %			
Steric	0.741	0.700	-
Electrostatic	0.259	0.300	0.230
Hydrophobic	-	-	0.487
H-bond donor	-	-	0.283
H-bond acceptor	-	-	-

[a]Standard error of prediction (SEP)
[b]Standard error of estimate (SEE)

CoMSIA analysis

Besides, the steric and electrostatic fields, CoMSIA was used to derive hydrogen bonding, donor, acceptor, and hydrophobic fields. The model is based on combining each filed with the others to evaluate their effects. Using the corresponding relevant q^2 and optimal component number, all 31 viable combinations were calculated (Figure 5). Figure 5 clearly shows that the highest q^2 (i.e. 0.580) is obtained at a point where all the electrostatic, hydrophobic, and hydrogen bond donor fields are presented. The outcome of the CoMSIA-derived model is presented in Table 2 indicating the model is capable of providing respective high q^2 and r^2 values of 0.580 and 0.752 for the optimum component number of 3. The derived statistical values from the model had a good bootstrap of 0.885, as well as group cross q^2 value of 0.550 and F = 34.361 with a low SEE of 0.201. The results

of each derived model in Table 2 are satisfactory. However, the r^2 value predicted by CoMSIA model (i.e. 0.670) exceeds those of CoMFA-1 (r^2 = 0.554) and CoMFA-2 (r^2 = 0.473) based models. The respective contributions of the electrostatic, hydrophobic, and hydrogen bond donor fields were shown to be 23.0%, 48.7%, and 28.3% by the model. The hydrophobic field in the CoMSIA model has a greater effect on the biological activity. The results of the CoMSIA model regarding electrostatic, hydrophobic, and hydrogen bond donor fields are presented in Figure 6. The pK$_i$ values predicted by the model are summarized in Table 1, and their correlation can be seen in Figure 3C.

Compound **2** was treated as the outlier in the best CoMFA and CoMSIA models, to decrease their predictive ability and all statistical parameters. The data in Table 1 indicate that compound **2** having the

maximum bio-activity (pK$_i$= 8.74) among the other compounds with the same series (i.e. compounds; **1**, **3**, **4**, **5**, and **6**) has a halogen in R$_3$ substituent. Comparing the experimental results obtained for molecules **3** and **4** with molecule **2** demonstrates that compound **3** (having Cl in R$_3$ substituent with pK$_i$= 7.79) and **4** (having F in R$_3$ substituent with pK$_i$= 7.80) did not show the significant biological activities, and using the halogen in this position would not cause any significant increase or decrease in biological activities. However, compound **2** due to its higher value

in contrast to molecules **3** and **4**, detected to be an outlier. Concerning the bulky characteristics in the R$_3$ substituent did not suggest the remarkable increase in biological activities (comparing molecules **5** with **6**). Therefore, the bulky characteristics of the Br group in this position would not be the reason for the dramatic increase of biological activities in molecule **2**. Hence, molecule **2** is treated as the outlier and omission of that from the data set compounds resulted in better r^2 values.
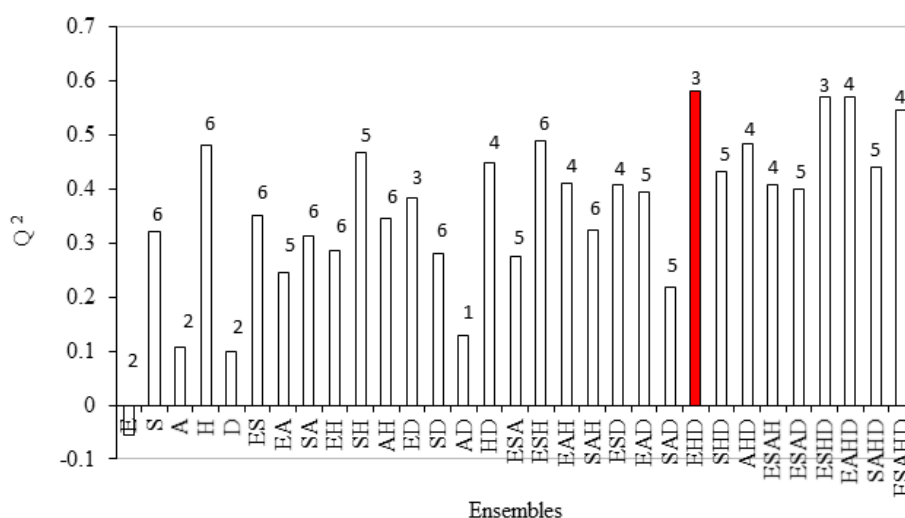

FIGURE 5 Graph of the 31 possible CoMSIA descriptors combinations (S=steric, E =electrostatic, H =hydrophobic, D/A=H-bond donor/acceptor) with their respective q^2 values, above bars reported their optimal number of components
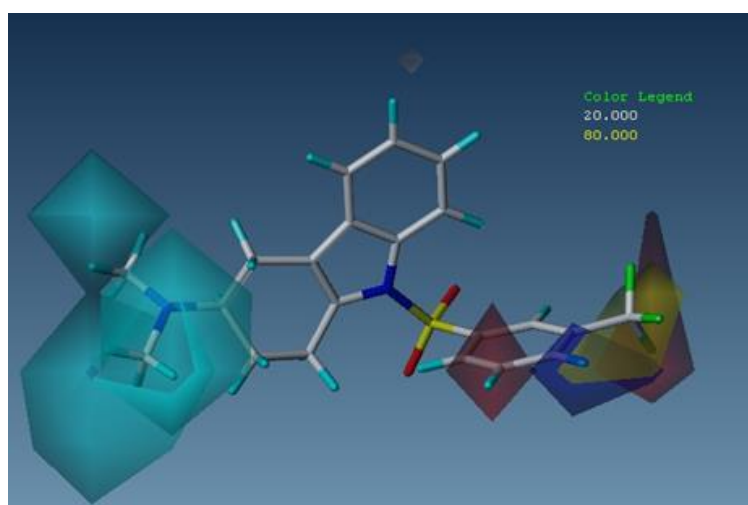

FIGURE 6 Contour maps of CoMSIA: electrostatic, hydrophobic, and H-bond donor fields based on compound 19

CoMFA contour maps

Figure 4 illustrates the steric and electrostatic contour maps given by the CoMFA model (after focusing regions) based molecule **19** as a reference. The regions with green contours represent that the bulkier groups (80% contribution) in these regions, could enhance of the biological activity. The yellow contours (20% contribution) show the regions in which the bulkier groups decrease bioactivity. Figure 4(A), illustrates the steric field effects, and indicates some regions the presence of bulky groups in which would enhance the bioactivity as well as regions where such bulky groups adversely influence bioactivity. The red and blue regions (Figure 4B) illustrate the CoMFA electrostatic contour maps. The regions in which electron-rich (electronegative) groups enhance bioactivity are exhibited by the red contours (20% contribution), while the blue (80% contribution) illustrate those where the bioactivity is boosted due to the increased positive (or decreased negative) charge. As provided in Figure 1, the reference molecule has been divided into 3 regions for a better presentation.

The steric contours of CoMFA (after region focusing) display three green areas near regions B and C at substituents of R_3, R_1, and R_2, respectively. The small contours in B at R_3 substituent illustrate the positive influence of bulky groups on the molecular bioactivity. Based the data presented in Table 1 and through the comparison of the activities in the series of molecules **6**, **5**, **1**, and **4** in which bulky groups (–SCH$_3$> -OCH$_3$> H > F) at R^3 substituent would enhance pKi (8.34 > 8.26 > 8.05 > 7.80), this can be explained. A similar effect can be noted in the case of molecules **36** and **37**, with **36**, including a Br atom and higher bioactivity (pK$_i$=8.12). In comparison, the less bulky molecule (**37**) had an F atom in region B at R^3 substituent and a pK$_i$ of 7.81. Furthermore, Table 1 indicates that the presence of bulky substituents (–OCH$_3$> Cl > F) in the same locations in molecules 9-11

enhances pK$_i$, i.e. **9** (with a –Cl group has pK$_i$=7.39), **10** (with an –F group has pK$_i$=7.36), and **11** (with an –OCH$_3$ group with pK$_i$=7.82). According to Table 1, the respective higher activities of (8.16 > 7.70 > 7.54) for **41**, **40**, and **39** could be attributed to the effects of –SCH$_3$, –OCH$_3$, –Br groups. This can be seen in molecules **21** (with a –Cl) and **20** (with a –Br group) where the presence of the bulky group (–Br > –Cl) would increase the pK$_i$ values (8.26 > 7.91).

To explain the green contours near C in R_1 and R_2 substituents, molecules **46** (with a –CH$_3$ group at R_2 in region C) and **48** (with an –H group at R_2 in region C) can be compared. Here the presence of the bulky group affected the pK$_i$ values (7.88> 7.41), and molecules **46** and **22**, in which case changing the group at R_1 substituent in region C from H to Me (H<Me), enhances the pK$_i$ from 7.88 to 8.43.

The steric contours map in Figure 4A is demonstrated by a small yellow contour at R_5 between 4 and 5 positions in A. The yellow contours in the vicinity of region A indicates the unfavorable influence of large groups on some compounds. In the light of the pK$_i$ values, the presence of large groups like –Br (molecule **8** with pK$_i$= 7.81) as opposed to –CH$_3$ (molecule **31** with pK$_i$= 8.08) at the 4-position of region A in the same series lowers the bioactivity. This fact can be described further by concerning molecules **3** (having H group) and **32** (having -CH$_3$ group) with molecule **9** (having Br group) where by increasing the size of groups at R_5 substituent (4-position) in region A (Br > CH3 > H), the pK$_i$ values are decreasing (7.39 < 7.79 < 7.74), namely.

Figure 4B indicates the increasing positive (or decreasing negative) charge enhanced bioactivity in the blue regions (80% contribution), whereas the opposite enhanced bioactivity in red regions (20% contribution). Figure 4 (B), clearly indicates two small blue contours around regions A and B. From the two, the one at the bottom of 4-position of R_5 substituent in region A was explained by

comparing molecules **31** and **12**, in which case replacing an -F group with -CH$_3$ enhanced the positive charge characteristic of the substituent and the pK$_i$ to 8.08 from 7.90. The same phenomenon was observed for molecules **34** and **15** and the pK$_i$ increase from 7.80 > 7.60, upon replacing (-F) with a methyl group. There is another small blue contour at the bottom of the R$_3$ substituent in region B. This can be understood by comparing molecules **1** (having –H group with pK$_i$= 8.05) and **4** (having –F group with pK$_i$= 7.80), **12** (having –H group with pK$_i$= 7.90) and **13** (having –F group with pK$_i$= 7.48) where using the negative charge group at this position would lead to decrease the pK$_i$ values. This fact is also observed in molecules **31**, **32**, and **33**, where increasing the negative charge feature (F > Cl > H) would result in a decrease of pK$_i$ values (7.49 < 7.74 < 8.08). Likewise, Figure 4 (B) demonstrated several large red contours near 2, 3, 5-positions of R$_5$ in region A. The large one close to position 2 of the substituent is clarified through a comparison of molecules **30**, **28**, and **5**. In this case, three electronegative groups, namely; F > Cl > H give rise to the respective bioactivities of 8.44 > 8.33 > 8.26. The set red contours in the proximity of position 3 of R$_5$ in region A is explained through studying molecules **19**, **16** and **1**, in which case the more electronegative where the CF$_3$ group with a higher electron withdrawing ability than chlorine and hydrogen group at 3- position of R$_5$ substituent in region A led to the maximal inhibition activity of 8.72 as opposed to 8.38 and 8.05 observed for chlorine and hydrogen.

CoMSIA contour maps

Figure 6 illustrates the results of the CoMSIA model in terms of the electrostatic, hydrophobic, and hydrogen bond donor fields, with the electrostatic field having a medium red contour at the bottom of A (5-position of R$_5$ substitutes) and region B (R$_4$ substitutes). To understand this the difference in the

behaviors of molecules **7** (with –F group and pK$_i$= 8.10) and **4** (with –H group and pK$_i$= 7.80) can be compared. In this case, an electronegative group in the bottom of R$_4$ substitutes resulted in an increase of pKi values. According to Figure 6, the CoMSIA model shows a large red contour close to position 3 of R$_5$ in A, which can be described by concerning molecules **16** and **1**. Replacing the Hydrogen with an electronegative group (-Cl) increased the negative charge behavior. Hence, the pKi value increased from 8.05 to 8.38. Figure 6 also shows a large blue contour close to position 4 of R$_5$ in region A, indicating the favorable effects of the presence of a positively charged on bioactivity. In the case of molecules **12** (with an –F group at position 4 of R$_5$ substituent in A) and **1** (with an –H group at 4 of R$_5$ substituent in region A) reveals that the presence of a highly electronegative group (F>H) decreases the pK$_i$ values from 8.05 to 7.90. This is further the case for molecules **14** and **35**, in which changing the methyl with a fluorine group, decreased the pK$_i$ from 8.23 to 7.61.

The hydrophobic contour maps can be seen in Figure 6. The yellow and white contours in the field, are areas in which the yellow indicates the presence of hydrophobic substituents, the sue of which enhances bioactivity (favored level 80 %). The white contours, on the other hand, show regions, the presence of hydrophobic groups in which lower bioactivity (unfavored level 20 %). The medium yellow contours close to positions 2 and 3 of R$_5$ substituent in region A can be seen in Figure 6. This can be realized through comparing molecules **28** and **5**, in which case boosting the hydrophobic character through replacing chlorine with hydrogen would result in increasing bioactivities (8.33 > 8.26). This fact is also seen in molecules **16** and **5**. In the case of these two molecules where enhancing the hydrophobic characteristic by replacing H with Cl increases bioactivity from 8.26 to 8.38. Reviewing the electrostatic and hydrophobic contours, indicates that position 3 of R$_5$ in

region A can show a higher biological activity when two characteristics are presented. Therefore, this is why the compound **16** (with a –Cl group at position 3 of R_5 substituent in A (pK_i= 8.38) has a stronger activity than molecule **28** (with a –Cl group at position 2 of R_5 in region A (pK_i =8.33)). The small white contours above the R_3 substituent in region B reflect the negative effect of hydrophobic groups on the biological activities, which can be better understood through studying molecules **16** and **17**. Replacing an -H group with -F, in this case, would increase the hydrophobic characteristic. Therefore, it leads to decrease the biological activity (8.38<8.30). This is further the case with molecules **25** and **23**. In this case, enhancing the hydrophobic characteristic by replacing -H with -F would lead to decrease the pK_i values (8.30 < 8.55). A similar effect can be observed in the case of molecules 1**9** and **21**, where using the group with a high hydrophobic activity (Cl > H) decreases pK_i from 8.75 to 7.91. Concerning Figure 6 and 4 (B), it can be observed that Figure 6 indicated the unfavorable effect of hydrophobic characteristic in R_3 substituent, and Figure 4 (B) demonstrated the favorable impact of hydrogen donor group in the same position. Comparing these effects reveal that the interaction of positively charged group and hydrophilic characteristic would lead to a higher binding affinity toward 5-HT_6 receptor. This effect can be seen in the case of molecules **5** and **1**, where changing hydrogen with an -OCH_3 group would increase the hydrophilic and positively charged group characteristics. Therefore, it results in a higher bioactivity (8.26> 8.05).

Figure 6 displays the hydrogen bond donor field, by cyan contours illustrating the areas where the presence of the donor group of hydrogen bond enhances bioactivity, whereas and the purple one illustrating the position in which the H-bond donor group lower this activity. Figure 6 includes two large cyan contours in region C enclosing to R_1 and R_2 substituents, which is understood through

comparing molecules **19**, **45**, and **47**, where increasing the activity of H-bond donor group in these positions (-$N(CH_3)_2$> -$NH(CH_3)$ > -NH_2) would lead to increase of biological activity (8.72 > 7.77 > 7.13), namely. As it can be seen in Table 1, in the case of molecules **22**, **46**, and **48**, boosting the H-bond donor group characteristic in these positions (-$N(CH_3)_2$> -$NH(CH_3)$ > -NH_2) with the same substituents would result in increasing the biological activity (8.43 > 7.88 > 7.41).

Molecular docking studies

To obtain further information about the interaction of the inhibitors with 5-HT_6 receptor with the structural properties of the active site of a receptor, and also appropriate conformation of ligand (inhibitors) with protein, docking technique was employed. The most active compound (**m19**) was docked in the active site of 5-HT_6 receptor, and the best conformation representing the lowest energy score was selected for the subsequent analyses. Therefore, the AutoDock 4.2 docking methods were used to look for the binding conformations of 5-HT_6 for the other inhibitors.

The results obtained from docking the most active compound (**m19**) with protein revealed that the inhibitor has the higher hydrophobic interactions with Tyr 191, Phe 208, Thr 118, Ala 117, Trp 265, Tyr268, Ile 189, Phe 212, Ala 269, Leu 125, Leu 216, Phe 261, Ala 272, and Met 207. These interactions were depicted in Figure 7 representing the significant impacts of hydrophobic features on enhancing the binding affinity. Figure 8 demonstrates the appropriate conformation of the compound with the maximum activity (**m19**) in the active site of 5-HT_6. In the light of this information, it can be concluded that increasing the total level of hydrophobic characteristics in molecular structures will provide a better binding affinity toward the 5-HT_6 receptor. As it can be visible from Figure 7 and Table 1, increasing the hydrophobic characteristics in R_5

substituent (metha position) in region A where a lot of oxygen moieties are provided by protein residues would result in better binding affinity. This is showing that the better binding affinity with appropriate conformation would happen when this position contains no atoms, which can provide hydrogen bond with Lys 296 and Glu 122. This fact can be seen in molecules **1** and **19**, **3**, **21**, **5**, and **22** where in each series by changing the R_5 substituent from hydrogen to CF_3 group (increasing the hydrophobic level), the binding affinity values were increased, respectively. This effect may be due to the lower number of interactions between ligand and inhibitor caused by hydrogen bond donor groups in contrast to hydrophobic groups in R_5 substituent. Comparing Figure 6 and 7 indicates that the CoMSIA contours map represents a blue contour in R_5 substituent (para position) where by considering the above assumption, this can be concluded that these contours are mostly referred to those atoms which are incapable of creating hydrogen bond. This influence can be perfectly understand concerning molecules **1** (with an -H group in the para site of R_5 substituent (pK$_i$

=8.05), **31** (having CH_3 group in para position of R_5 substituent with pK$_i$ value of 8.08), and **38** (having OCH_3 group in para position of R_5 substituent with pK$_i$ value of 7.69) where using the $-OCH_3$ would result in creating hydrogen bond with Cys 167, while using $-CH_3$ and H groups would lead to eliminate the crucial H-bond interactions, and subsequently increase hydrophobic levels and create the higher interactions with Thr 118, Iel 189, and Ala 117.

To better realize various interactions of the molecule with the maximum activity (**m19**) with a receptor, the two-dimensional representation of the interactions were generated using Ligandscout 3.03. Figure 9 illustrates the results obtained by Ligandscout 3.03. A total number of 15 hydrophobic interactions was formed between compound 19 and 5-HT$_6$ receptor (Tyr 191, Phe 208, Thr 118, Ala 117, Trp 265, Tyr268, Ala 292, Ile 189, Phe 212, Ala 269, Leu 125, Leu 216, Phe 261, Ala 272, and Met 207). Therefore, it can be concluded that the residues have a key role in the inhibition properties of 5-HT$_6$, based on the structural analyses and study of the hydrophobic interactions.
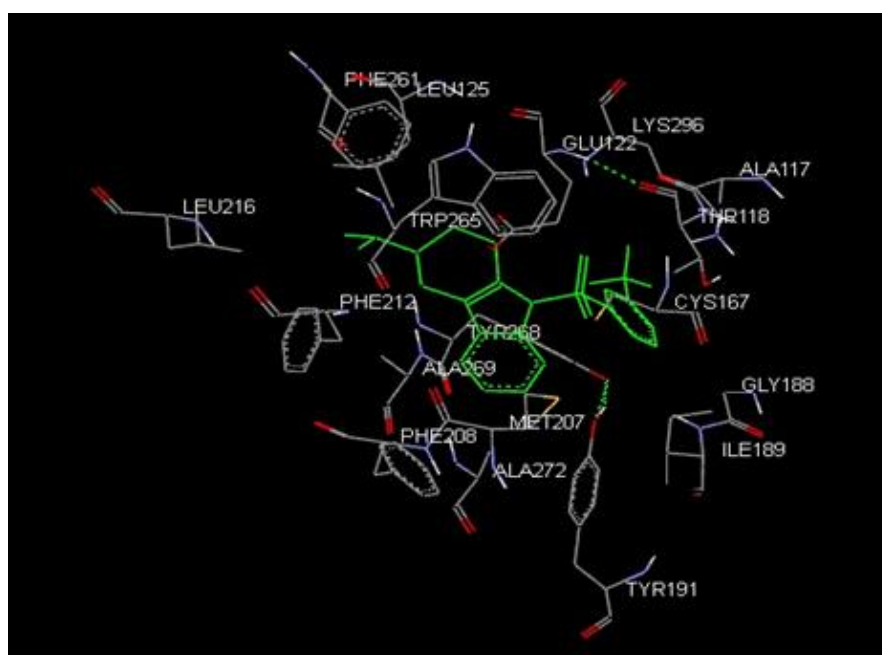

FIGURE 7 Binding pocket of 5-HT$_6$ bound to compound 19 (green). Hydrogen bonds are marked as green dashed lines
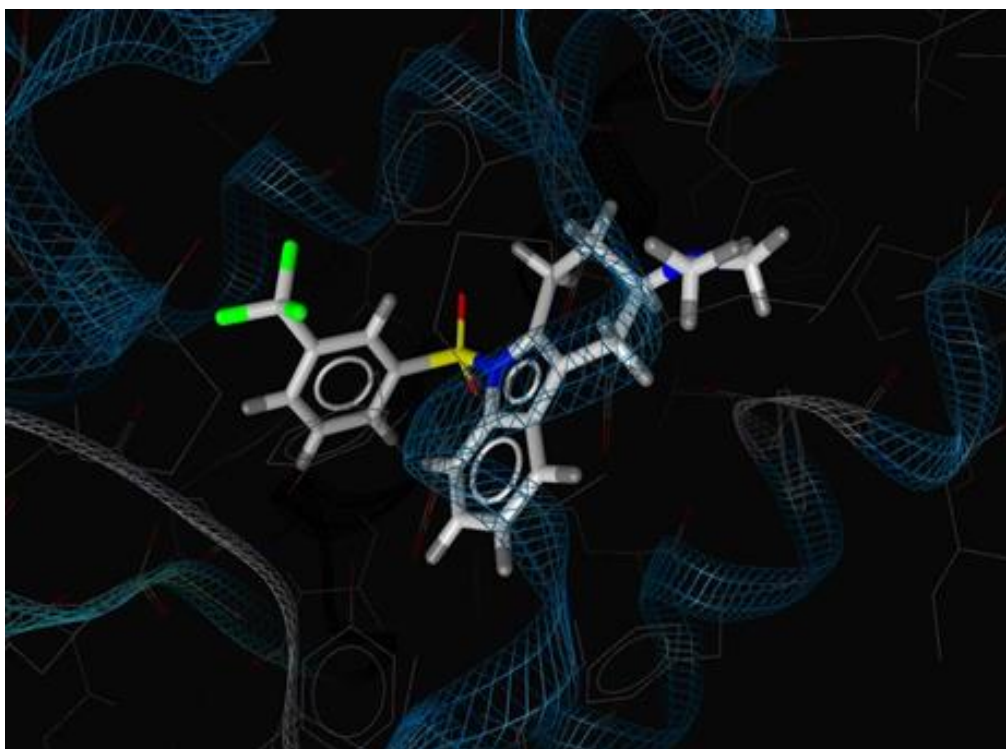
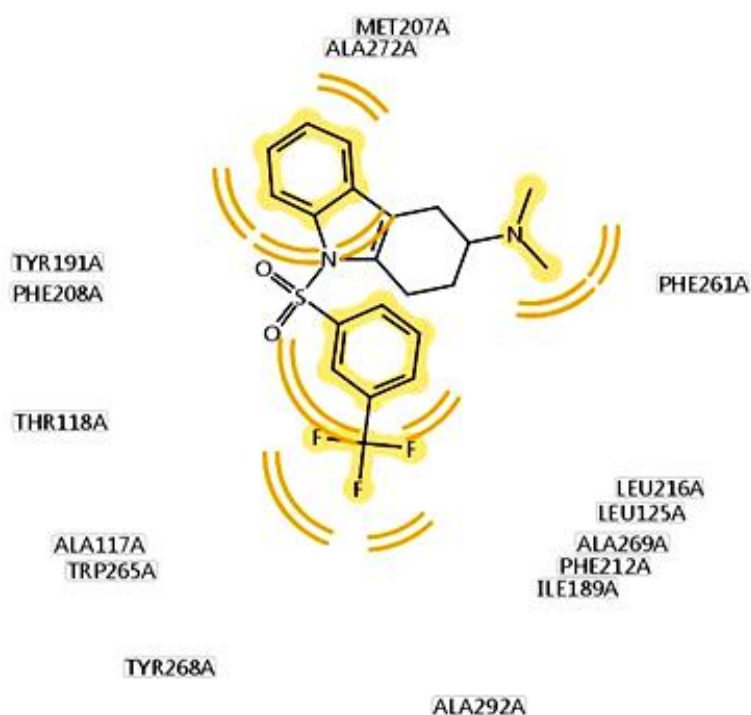**FIGURE 8** Hit molecule position in the active site of protein and its appropriate orientation

FIGURE 9 The 2D structure of interactions between lignad and receptor sketched by LigandScout 3.03 program

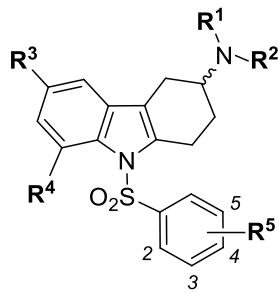*Design of new 5-HT$_6$ receptor inhibitors*

According to the contours maps derived by models (CoMFA and CoMSIA), and docking results, some important information was presented on the effect of each group as a substituent for region A, B, and C. In the light of the data, the novel highly active molecules

were designed as 5-HT$_6$ inhibitors and listed in Table 3. Through the analysis of contours map produced by each of the models, enhanced bioactivity levels can be obtained by adjusting the roles of bulky and H-bond donor groups in region C. The results indicate that the negative charge group with the higher hydrophobic features in region A can improve the bioactivity. Yet, the hydrophobic properties in R$_3$ substituent of region B should be lowered. The bulky group in *para*-position of R$_5$ substituent in region A can lead to the higher biological activities. The better biological activities can also be achieved where the negative charge atom used as the R$_4$ substituent in region B. Molecular docking analysis could reveal that the main interaction between the most potent inhibitor and 5-HT$_6$ receptor is a hydrophobic characteristic. Concerning the CoMSIA model and its contours contributions, it can be observed that CoMSIA model represented a higher contribution for the hydrophobic levels. This is in line with those founds simulated by molecular docking methodology. Since the statistical results (higher r^2_{test} and less optimal number of components) obtained for CoMSIA model were more appropriate than those obtained by CoMFA-1 and CoMFA-2 models, the pK$_i$ values were predicted by CoMSIA model, and according to the data in Table 3, all new designed compounds could provide higher pK$_i$ values as 5-HT$_6$ inhibitors.

TABLE 3 Chemical structures of 5-HT$_6$ receptor inhibitors and predicted pK$_i$ values of newly designed compounds

No.	Substituents					Predicted activity CoMSIA
	R$_1$	R$_2$	R$_3$	R$_4$	R$_5$	

No.	R$_1$	R$_2$	R$_3$	R$_4$	R$_5$	Predicted activity CoMSIA
19	CH$_3$	CH$_3$	H	H	3-CF$_3$	8.53
N1	CH$_3$	CH$_3$	CH3	CH$_3$	3-CF$_3$	8.58
N2	CH$_3$	CH$_3$	H	CH$_3$	3-CF$_3$	8.57
N3	CH$_3$	CH$_3$	CH$_3$	H	3-CF$_3$	8.92
N4	CH$_3$	CH$_3$	CH$_3$	CH$_3$	3-Phenyl	8.61
N5	CH$_3$	CH$_3$	H	CH$_3$	3-Phenyl	8.61
N6	CH$_3$	CH$_3$	CH$_3$	H	3-Phenyl	8.76
N7	CH$_3$	CH$_3$	H	H	3-Phenyl	8.76
N8	CH$_3$	CH$_3$	CH$_3$	CH$_2$CH$_3$	3-Phenyl	8.59
N9	CH$_3$	CH$_3$	CH$_3$	*i*Pr	3-CF$_3$	8.60
N10	CH$_3$	CH$_3$	H	H	3-CH$_3$	8.54
N11	CH$_3$	CH$_3$	H	H	3- 3,5-CH$_3$Ph	8.78
N12	CH$_3$	CH$_3$	H	CH$_3$	3- 3,5-CH$_3$Ph	8.66
N13	CH$_3$	CH$_3$	H	CH$_2$CH$_3$	3- 3,5-CH$_3$Ph	8.56
N14	CH$_3$	CH$_3$	H	Pr	3- 3,5-CH$_3$Ph	8.64
N15	CH$_3$	CH$_3$	H	H	3- 3,5-CF$_3$Ph	8.74
N16	CH$_3$	CH$_3$	H	CH$_3$	3- 3,5-CF$_3$Ph	8.66
N17	CH$_3$	CH$_3$	H	Phenyl	3- 3,5-CF$_3$Ph	8.67
N18	CH$_3$	CH$_3$	H	CH$_2$CF$_3$	3- 3,5-CF$_3$Ph	8.74

Conclusion

The study involved developing CoMFA, CoMSIA, and 3D-QSAR models along with docking methodology to discover the role of various substituents in different regions for the range of molecules as 5-HT$_6$ receptor inhibitors and the appropriate conformation of ligand with 5-HT$_6$ receptor, respectively. Using PLS analysis, the correlations of CoMFA and CoMSIA descriptors with bioactivity levels were determined. The determined statistical factors namely q^2, r^2, F, and bootstrap were high except for low SEEs, which reflected the acceptable prediction capability of the 3D-QSAR models. The external prediction capability of each model was also validated by evaluating a test set of 9 molecules. The CoMFA and CoMSIA based data reflected the effects of steric, electrostatic, hydrophobic, and hydrogen bond donor fields on the aligned molecules. Cumulatively, the large group with higher H-bond donor characteristic available in region C can lead to the higher bioactivity levels. Furthermore, highly electronegative charge groups, which have higher hydrophobic characteristics in region A can lead to a better bioactivity. However, it was observed that the most effective substitute in terms of enhancing the bioactivity of 5-HT$_6$ receptor inhibitors in region A is meta and para positions, and in region C is R$_1$ and R$_2$ positions. Molecular docking analysis along with CoMSIA model could reveal the significant role of hydrophobic characteristic on increasing the inhibitors potency. Concerning the derived information would provide a better insight to design the new inhibitors with improvement in their pK$_i$ values.

Acknowledgements

Conflict of Interest

The authors declare no conflict of interests.

Orcid:

Eslam Pourbasheer:
https://www.orcid.org/0000-0001-8969-4341

References

[1] C. Gerard, S. El Mestikawy, C. Lebrand, J. Adrien, M. Ruat, E. Traiffort, M. Hamon, M.P. Martres, *Synapse*, **1996**, *23*, 164-173. [Crossref], [Google Scholar], [Publisher]

[2] P. Hartig, N. Adham, J. Bard, A. Hou-yu, H. T. Kao, M. Macchi, L. Schechter, D. Urquhart, J. Zgombick, M. Durkin, R. Weinshank, T. Branchek, in Serotonin, eds. P.M. Vanhoutte, P.R. Saxena, R. Paoletti, N. Brunello, A.S. Jackson, *Springer Netherlands*, **1993**, *5*, 21-31. [Crossref], [Google Scholar], [Publisher]

[3] F.J. Monsma, Y. Shen, R.P. Ward, M.W. Hamblin, D.R. Sibley, *Mol. Pharmacol*, **1993**, *43*, 320-327. [Crossref], [Google Scholar], [Publisher]

[4] R.P. Ward, M.W. Hamblin, J.E. Lachowicz, B.J. Hoffman, D.R. Sibley, D.M. Dorsa, *Neuroscience*, **1995**, *64*, 1105-1111. [Crossref], [Google Scholar], [Publisher]

[5] T.A. Branchek, T.P. Blackburn, *Annu. Rev. Pharmacol. Toxicol.*, **2000**, *40*, 319-334. [Crossref], [Google Scholar], [Publisher]

[6] K.G. Liu, A.J. Robichaud, *in International Review of Neurobiology, ed. B. Franco, Academic Press*, **2010**, *94*, 1-34. [Crossref], [Google Scholar], [Publisher]

[7] J.M. Palacios, *Pharmacological Sciences: Perspectives for Research and Therapy in the Late 1990s, eds. A.C. Cuello and B. Collier, Birkhäuser Basel*, **1995**, *3*, 17-27. [Crossref], [Google Scholar], [Publisher]

[8] J. Scharfetter, Psychopharmacogenetics, eds. P. Gorwood, M. Hamon, Springer US, **2006**, *5*, 101-148. [Crossref], [Google Scholar], [Publisher]

[9] M. Ramírez, *Alz. Res. Therapy*, **2013**, *5*, 1-8. [Crossref], [Google Scholar], [Publisher]

[10] N. Upton, T.T. Chuang, A.J. Hunter, D.J. Virley, *Neurotherapeutics*, **2008**, *5*, 458-469. [Crossref], [Google Scholar], [Publisher]

[11] R. Westkaemper, B. Roth, *The Serotonin Receptors, ed. B. Roth, Humana Press*, **2006**, *2*, 39-58. [Crossref], [Google Scholar], [Publisher]

[12] B. Grimaldi, A. Bonnin, M.-P. Fillion, M. Ruat, E. Traiffort, G. Fillion, *N-S Arch Pharmacol*, **1998**, *357*, 393-400. [Crossref], [Google Scholar], [Publisher]

[13] R. Schreiber, A. Sleight, M. Woolley, *The Serotonin Receptors, ed. B. Roth, Humana Press*, **2006**, *17*, 495-515. [Crossref], [Google Scholar], [Publisher]

[14] A.V. Ivachtchenko, E.B. Frolov, O.D. Mitkin, V.M. Kysil, A.V. Khvat, I.M. Okun, S.E. Tkachenko, *Bioorg. Med. Chem. Lett.*, **2009**, *19*, 3183-3187. [Crossref], [Google Scholar], [Publisher]

[15] A.V. Ivachtchenko, E.S. Golovina, M.G. Kadieva, A.G. Koryakova, O.D. Mitkin, S.E. Tkachenko, V.M. Kysil, I. Okun, *Eur. J. Med. Chem.*, **2011**, *46*, 1189-1197. [Crossref], [Google Scholar], [Publisher]

[16] A.V. Ivachtchenko, E.S. Golovina, M.G. Kadieva, V.M. Kysil, O.D. Mitkin, A.A. Vorobiev, I. Okun, *Bioorg. Med. Chem. Lett.*, **2012**, *22*, 4273-4280. [Crossref], [Google Scholar], [Publisher]

[17] R.V.S. Nirogi, J.B. Konda, R. Kambhampati, A. Shinde, T.R. Bandyala, P. Gudla, K.K. Kandukuri, P. Jayarajan, V. Kandikere, P.K. Dubey, *Bioorg. Med. Chem. Lett.*, **2012**, *22*, 6980-6985. [Crossref], [Google Scholar], [Publisher]

[18] E. Pourbasheer, R. Aalizadeh, M. R. Ganjali, *Arab. J. Chem.*, **2019**, *12*, 2141-2149. [Crossref], [Google Scholar], [Publisher]

[19] S. Riahi, M.R Ganjali, P. Norouzi, F. Jafari, *Sens. Actuator. B Chem.*, **2008**, *132*, 13-19. [Crossref], [Google Scholar], [Publisher]

[20] E. Pourbasheer, R. Aalizadeh, J. Saffar-Ardabili, M.R Ganjali, *J. Mol. Liq.*, **2015**, *204*, 162-169. [Crossref], [Google Scholar], [Publisher]

[21] E. Pourbasheer, S. Riahi, M.R. Ganjali, P. Norouzi, *Mol. Divers*, **2011**, *15*, 645-653. [Crossref], [Google Scholar], [Publisher]

[22] H. Rafiei, M. Khanzadeh, S. Mozaffari, M.H. Bostanifar, Z.M. Avval, R. Aalizadeh, E. Pourbasheer, *Excli J.*, **2016**, *15*, 38-53. [Crossref], [Google Scholar], [Publisher]

[23] E. Pourbasheer, S. Ahmadpour, R. Zare-Dorabei, M. Nekoei, *Arab. J. Chem.*, **2017**, *10*, 33-40. [Crossref], [Google Scholar], [Publisher]

[24] M. Nekoei, M. Mohammadhosseini, E. Pourbasheer, *J. Chin. Chem. Soc.*, **2021**, *68*, 1972-1986. [Crossref], [Google Scholar], [Publisher]

[25] M.J. Islam, A. Kumer, S. Paul, M.N. Sarker. *T. Chem. Method.*, **2020**, *4*, 130-142. [Crossref], [Google Scholar], [Publisher]

[26] F. Fratev, E. Benfenati, *J. Chem. Inf. Model.* **2005**, *45*, 634-644. [Crossref], [Google Scholar], [Publisher]

[27] A.J. Hopfinger, S. Wang, J.S. Tokarski, B. Jin, M. Albuquerque, P.J. Madhav, C. Duraiswami, *J. Am. Chem. Soc.*, **1997**, *119*, 10509-10524. [Crossref], [Google Scholar], [Publisher]

[28] Q.S. Du, J. Gao, Y.T. Wei, L.Q. Du, S.Q. Wang, R.B. Huang, *J. Chem. Inf. Model.*, **2012**, *52*, 996-1004. [Crossref], [Google Scholar], [Publisher]

[29] P. Tosco, T. Balle, *J. Chem. Inf. Model.*, **2011**, *52*, 302-307. [Crossref], [Google Scholar], [Publisher]

[30] E. Pourbasheer, R. Aalizadeh, S. S. Tabar, M.R. Ganjali, P. Norouzi, J. Shadmanesh, *J. Chem. Inf. Model.*, **2014**, *54*, 2902-2914. [Crossref], [Google Scholar], [Publisher]

[31] R.D. Cramer, D.E. Patterson, J.D. Bunce, *J. Am. Chem. Soc.*, **1988**, *110*, 5959-5967. [Crossref], [Google Scholar], [Publisher]

[32] G. Klebe, U. Abraham, T. Mietzner, *J. Med. Chem.*, **1994**, *37*, 4130-4146. [Crossref], [Google Scholar], [Publisher]

[33] E. Pourbasheer, R. Aalizadeh, *Sar Qsar Environ. Res.*, **2016**, *27*, 385-407. [Crossref], [Google Scholar], [Publisher]

[34] E. Pourbasheer, S.S. Tabar, V.H. Masand, R. Aalizadeh, M.R. Ganjali, *Sar Qsar Environ. Res.*, **2015**, *26*, 461-477. [Crossref], [Google Scholar], [Publisher]

[35] H.T. Manual, SYBYL 7.3. In: St. Louis, Missouri, USA Tripos International, **2006**. [Publisher]

[36] M. Clark, R.D. Cramer, N. Van Opdenbosch, *J. Comput. Chem.*, **1989**, *10*, 982-1012. [Crossref], [Google Scholar], [Publisher]

[37] J. Gasteiger, M. Marsili, *Tetrahedron*, **1980**, *36*, 3219-3228. [Crossref], [Google Scholar], [Publisher]

[38] E. Pourbasheer, R. Bazl, M. Amanlou, *Med. Chem. Res.*, **2014**, *23*, 2252-2263. [Crossref], [Google Scholar], [Publisher]

[39] O.O. Adeboye, F.O. Oyeleke, S.A. Agboluaje, *Adv. J. Chem. A.*, **2022**, *5*, 147-163. [Crossref], [Google Scholar], [Publisher]

[40] S.A. Ahmed, S. Salau, A. Khan, M. Saeed, Z. Ul-Haq, *Adv. J. Chem. A*, **2022**, *5*, 226-240. [Crossref], [Google Scholar], [Publisher]

[41] G.M. Morris, R. Huey, W. Lindstrom, M.F. Sanner, R.K. Belew, D.S. Goodsell, A.J. Olson, *J. Comput. Chem.*, **2009**, *30*, 2785-2791. [Crossref], [Google Scholar], [Publisher]

[42] T. Okada, M. Sugihara, A.N. Bondar, M. Elstner, P. Entel, V. Buss, *J. Mol. Biol.*, **2004**, *342*, 571-583. [Crossref], [Google Scholar], [Publisher]

[43] G. Wolber, T. Langer, *J. Chem. Inf. Model.*, **2004**, *45*, 160-169. [Crossref], [Google Scholar], [Publisher]

[44] G. Folkers, A. Merz, D. Rognan, ed. H. Kubinyi, ESCOM, Leiden, the Netherlands, 1993, 583-618. [Crossref], [Google Scholar], [Publisher]

[45] V.N. Viswanadhan, A.K. Ghose, G.R. Revankar, R.K. Robins, *J. Chem. Inform. Comput. Sci.*, **1989**, *29*, 163-172. [Crossref], [Google Scholar], [Publisher]

[46] S. Wold, A. Ruhe, H. Wold, I. Dunn, W. Siam, *J. Sci. Stat. Comput.*, **1984**, *5*, 735-743. [Crossref], [Google Scholar], [Publisher]

[47] B. Bush, R. Nachbar Jr., *J. Computer-Aided Mol. Des.*, **1993**, *7*, 587-619. [Crossref], [Google Scholar], [Publisher]

[48] Y.C. Martin, P. Willett, *Designing Bioactive Molecules: Three-Dimensional Techniques and Applications American Chemical Society, Washington DC*, **1998**. [Google Scholar], [Publisher]